Electronic Supplementary Material (ESI) for RSC Advances

Magnetic domains in rolled-up nanomembranes of Co/Pt multilayers with perpendicular magnetic anisotropy

J. Zarpellon,[a,b] H. F. Jurca,[a,c] J. Varalda,[a] C. Deranlot,[d] J. M. George,[d] M. D. Martins,[e] S. O. Parreiras,[e] C. Müller,[a,f] and D. H. Mosca[a*]

[a] *Laboratório de Nanoestruturas para Sensores, Universidade Federal do Paraná, Centro Politécnico, Caixa Postal 19091, 81531-990 Curitiba, Brazil*

[b] *Instituto Federal do Paraná - Campus Paranaguá - Rua Antônio Carlos Rodrigues 453 - Porto Seguro, 83215-750 Paranaguá, Brazil*

[c] *Instituto Federal do Paraná – Campus Irati – Rua Pedro Koppe, 100 – Vila Matilde, 8400-500 Irati, Brazil*

[d] *Unité Mixte de Physique CNRS–Thales and Université Paris-Sud, Campus de Polytechnique, 1, Avenue Augustin Fresnel, 91767, Palaiseau, Cedex France*

[e] *Laboratório de Nanoscopia, Centro de Desenvolvimento da Tecnologia Nuclear, 31270-901 Belo Horizonte, MG, Brazil*

[f] *Technische Universität Chemnitz, 09107, Chemnitz, Germany*

* Corresponding author e-mail address: mosca@fisica.ufpr.br

Abstract

Compact rolled-up nanomembranes of high quality (111)-oriented Co/Pt multilayers with perpendicular magnetic anisotropy are realized by combining strain engineering with top-down preparation methods. Magnetic force microscopy analyses were performed in the demagnetized state and under magnetic fields applied on rolled-up Co/Pt tubes. Observed magnetic domains are composed of radially polarized stripe-shaped domains. The stripes running along the rolled-up tubes axis are observed for magnetic fields applied along this direction, whereas a salmon-like pattern is observed for magnetic fields applied along the tube diameter. Present results have potential for applications ~~nanoscale~~ as magnetic encoder and servo motors. ~~and other small and powerful microdevices where high magnetic flux densities are required~~.

Electronic Supplementary Material (ESI) for RSC Advances

Introduction

Nanosized magnetic structures such as dots, wires, and cylinders have been studied for fundamental and technological interest [1-3]. Both their magnetic behaviors and internal magnetic states have potential for applications in magnetic memories, sensors and logical devices [4]. Particularly, ferromagnetic tubes are considered as candidates for microdevices as magnetic encoder and servo-motors and in microfluidic biomedical devices because the floatability in the liquids due to its inner empty spaces [5,6].

In the last decade, it was demonstrated that rolled-up nanotechnology can be used to transform nanomembranes into compact three dimensional architectures of predetermined size and geometry [7,8]. The fabrication process is fully integrative, providing rolled-up magnetic tubes of high quality and aspect ratio. Rolled-up nanotechnology has been successfully used for the development of various devices on chip such as cell culture scaffolds [9,10], compact electrical components [11-14], microfluidic systems [15] and optical resonators [16–19]. Nevertheless, developments which consider the integration of magnetic materials into rolled-up components are rare. Initially, rolled-up permalloy microtubes were fabricated and demonstrated as a microfluidic sensor to measure viscosity [20]. Later, rolled-up Fe_3Si [21] and Co [22] nanomembranes as well as coiled Co [23] and Co–Pt strips [24] have been investigated concerning structural and magnetic properties. More recently, rolled-up microtubes have been fabricated for the study of spinwave interference [25] and magnetoresistance [26–29] e.g. for the detection of magnetic objects [26]. However, the investigation of magnetic domain configurations in rolled-up tubes are is quite rare [30].

In this letter we investigate the local magnetic domain configurations in micrometer long rolled-up Co/Pt nanomembranes which behaves as radially polarized cylindrical magnets due to perpendicular magnetic anisotropy (PMA) [31].

Experimental

Co/Pt multilayered films were grown by magnetron sputtering at room temperature (base pressure of about 5×10^{-8} mbar) on two templates. First, a series of samples dedicated to magnetization measurements were grown on a thermally oxidized Si(001) wafer, where a 20-nm-thick (111)-oriented face-centered cubic Pt layer was used as buffer. The deposited multilayers (MLs) consists of SiO_2/Pt(20 nm)/[Co(0.6 nm)/Pt(1.0 nm)]$_5$/Au(10 nm), where a 10-nm-thick Au capping layer is used to avoid detrimental effects due to the atmospheric air exposure. Cross-sectional transmission electron microscopy (TEM) analysis was performed to study the structure and stacking of the layers.

A second series of samples was prepared to fabricate rolled-up (Co/Pt) microtubes combining conventional photolithography and sputter deposition. First, photoresist (ARP-3510 positive resist) with a thickness of approximately 2 μm on SiO_2 was patterned into 225 squares of 50 × 50 μm^2 size. Next, a multilayered structure consisting of Pt(10 nm)/[Co(0.6 nm)/Pt(1.0 nm)]$_5$/Pt(2.0 nm) was deposited by sputtering onto the photoresist layer. Co/Pt multilayer with above mentioned layer thickness typically exhibit uniaxial magnetic anisotropy K_u that directs the easy axis of magnetization perpendicular to the film plane, as recently reported [32]. Magnetization measurements using a Vibrating Sample Magnetometer (VSM) were used to confirm that planar samples grown on photoresist present PMA. Finally, the Pt(10 nm)/[Co(0.6 nm)/Pt(1.0 nm)]$_5$/Pt(2.0 nm) MLs were rolled-up by dissolving the photoresist with pure acetone, resulting in microtubes. Scanning Electron Microscopy (SEM) were performed to characterize the uniformity and outer rolling edge of a Co/Pt microtube. In order to avoid collapse of the rolled up structures due to capillary forces, the organic solution was removed afterward using a supercritical dryer (Bal-Tec CPD 030). Applying this procedure, only the rolled up tubes remain on the SiO_2 substrate.

To analyze the magnetic domain configurations of these microtubes, Magnetic Force Microscopy (MFM) images were made for samples in both the demagnetized states and with magnetic field applied parallel to the rolled-up microtube axis or tube diameter. MFM measurements were performed using a NTEGRA Aura MFM (NT-MDT Co.) in the standard double pass dynamic mode. The phase shift of cantilever oscillations under a gradient of magnetic field was registered as the MFM contrast. Hard-magnetic-coated silicon cantilevers (MFMR, Nanosensors™) magnetized along the tip axis prior to magnetic imaging was used in the MFM experiments.

Electronic Supplementary Material (ESI) for RSC Advances

Results and discussion

Co/Pt MLs consisting of five chemically well-defined bilayers Co(0.6 nm)/Pt(1.0 nm) were described elsewhere [32]. Hysteresis loops of MLs on photoresist were measured using VSM with magnetic field applied perpendicular and parallel to the sample plane. Clearly, these samples exhibit PMA, as shown in Figure 1(a). SEM image showing the uniformity of diameter of the one rolled-up micro-tube prepared with sample is shown in Figure 1(b).

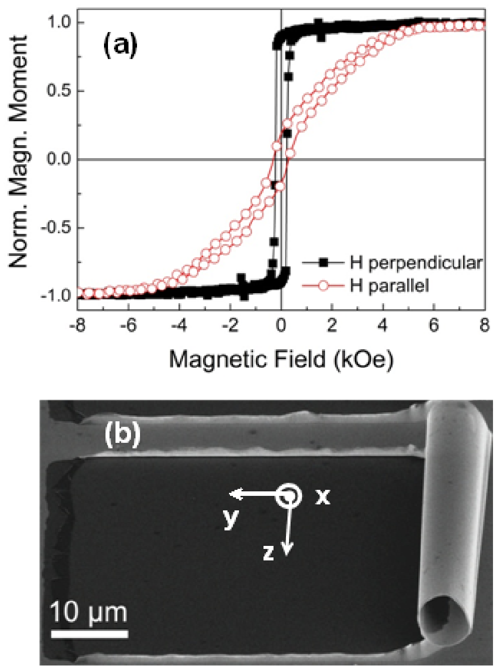

Figure 1: (color online) (a) VSM hysteresis loops measured at 300 K for Pt(10 nm)/[Co(0.6 nm)/Pt(1.0 nm)]$_5$/Pt(2.0 nm) MLs on photoresist with magnetic field applied parallel and perpendicular to the substrate. (b) SEM image of the outer rolling edge of a rolled-up microtube having a diameter of about 6 µm. The coordinate system refers to the applied field orientations, being the x axis out of plane.

Figure 2 summarizes the AFM topography images and MFM images in the demagnetized state (obtained by decreasing the magnetic field from 5 kOe to zero in a oscillation mode), taken from the same sample regions. To facilitate the visualization of magnetic domains we have adopted the convention of respectively showing horizontal and vertical tube sections for magnetic fields applied parallel and perpendicular to the tube axis.

The magnetic domain patterns in the MFM images can be classified as multidomain with a mixture of bands and bubbles domains. Figure 2(a) and (b) correspond to the measurements on the film after demagnetization with a perpendicular field, while Figures 2(c)-(d) and (e)-(f) are related to the measurements on the microtube with

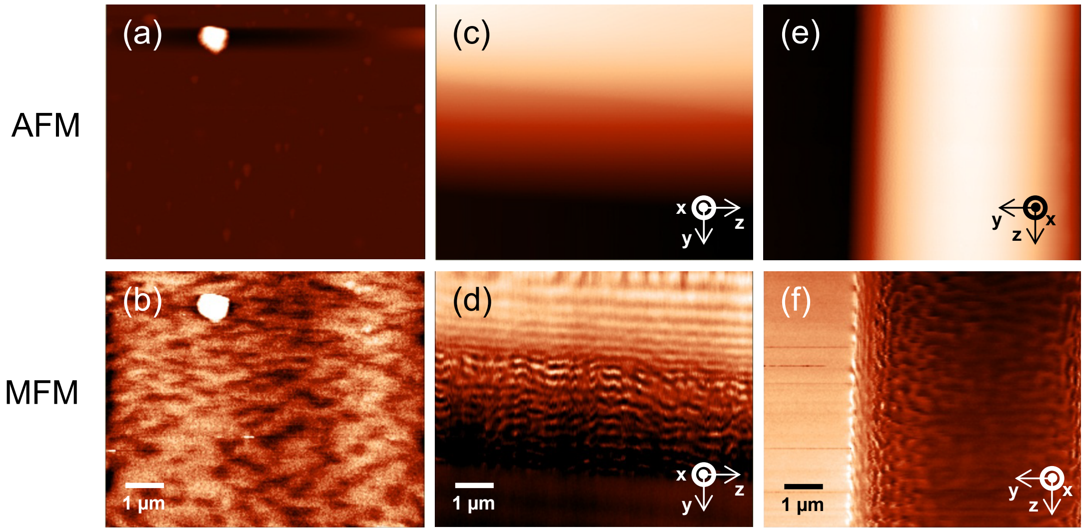

demagnetization field parallel and perpendicular to the tube axis, respectively.

Figure 2: (color online) AFM and MFM images of the same flat regions of the film (a,b) and sections of rolled-up membranes of multilayered film with tubes aligned horizontally (c,d) and vertically (e,f). MFM images were scanned in the demagnetized states which were obtained by decreasing the magnetic field from 5 kOe to zero in a oscillation mode, along: (b) the film normal, (d) tube axis (z axis), and (f) tube diameter (y axis). All images areas are 8 µm x 10 µm.

The mixture pattern consisting of perpendicular magnetization upward and downward observed in the film is probably a result of stress induced by the photoresist layer.It is known that this kind of stress may change the magnetic anisotropy in the film plane

[22]. Wound-up patterns with radial magnetization inward and outward are observed in the rolled-up tube, as shown in Figures 2(d) and (f). Band domains extended along the tube axis or diameter, according to the orientation of demagnetizing field (along the z and y axis, respectively). This indicates a kind of second-order stripe nucleation, which commonly occurs when the demagnetizing field is applied parallel to the easy magnetization axis. In the case of rolled-up tubes, the PMA of Co/Pt multilayers favors a radial easy axis, while the geometry favors an uniaxial anisotropy along the tube axis [21, 22, 33]. These two contributions create a competition between the PMA of multilayers and the shape anisotropy to establish the easy axis of magnetization of the microtubes. The peculiar wound-up patterns probably arise due to the stability of stripe domains characteristic of samples with PMA.

An early theory pioneered by Kittel [34, 35], which is still held widely today, predicts that most basic stripe domain structures have three competing energy terms: surface energy σ of the domain walls, magnetic field energy associated with building the configuration of magnetic poles in the sample, and anisotropy energy of magnetization orientation. The stripe domains are formed by minimizing the total energy density of the domain structure. In a simplified form, a thin film of ferromagnetic material with PMA having thickness L and consisting of unlimited long parallel domains of periodic laminar structure (stripes) with same widths $W^{\pm}$, whose magnetization is the same in magnitude but reverses orientation $\pm M_S$ from domain to domain, gives a dependence of $W^{\pm} = 0.8\ (\sigma L/M_S^2)^{1/2}$. A transition between a stripe-shaped domain structure and uniform domain structure with PMA is expected to occur. A critical condition to annihilation of stripe domains is reached at a field identical with the anisotropy field $H_K = 2K_u/M_S$, which in our case is 4 kOe (not shown). Such a field value is much higher than the maximum field available in our MFM experiments.

MFM images scanned at a field of 500 Oe applied parallel to the tube axis and parallel to tube diameter are shown in Fig. 3(a) and (b) (z and y axis, respectively). Stripe domains are observed longitudinally to the tube axis in Figure 3(a), whereas peculiar fingerprint domains resembling salmon-like pattern are observed for field applied along the tube diameter in Figure 3(b). The MFM tip probes only the stray field $\boldsymbol{B}_{stray}$ and the magnetic interacting force is given by ½($\boldsymbol{m}_{tip}$·$\boldsymbol{B}_{stray}$), where $\boldsymbol{m}_{tip}$ is the magnetic moment of the MFM tip. In the case of microtubes, the tip probes only the radial component of $\boldsymbol{B}_{stray}$, indicating that the stripe-shaped domains shown in the MFM images are formed by alternating stray fields directed radially inward and outward. Considering the three-dimensional field solution for radially polarized permanent-magnet with cylindrical geometry [36], the Co/Pt microtubes have a radial magnetization with radial component. The $\boldsymbol{B}_{stray}$ in the center of each stripe is proportional to saturation magnetization of Co/Pt, i.e., each stripe is presumably radially magnetized with $\pm Ms$. Microtubes with this type of magnetization are quite rare, giving rise a high flux density. Most of works reveals magnetization reversal of microtubes with planar magnetization exhibiting vortex and transversal configurations [37-40].

Another interesting feature is the salmon-like domains observed in Figure 3(b) for the case with magnetic field applied perpendicular to tube axis. This pattern is probably connected to additional mechanical stress produced by the applied magnetic field (along y axis) that can induce small changes in the tube geometry and deviations from the ideal tubular geometry. A stress pattern resembling a fingerprint was already observed [35] and can be created or destroyed in a sample by an external field. In Co/Pt microtubes, a stress pattern is expected to occur if occur an imbalance of radial magnetizations along the x direction on the upper and lower pole surfaces of the tube. It may generate opposite shear forces along z axis due to magnetic torque, while no force will act in the y-axis surfaces. Consequently, when an external field is applied along the microtube diameter, a stress is induced and a slight deviation from the symmetrical radial anisotropy may occur. This is equivalent to a tilt on the anisotropy axis, resulting in a salmon-like domain pattern as observed in Figure 3(b). Larger period and amplitude of salmon-like bands is therefore an indication of the tube geometry distortion. Figure 3(b) also show stripes on the flat surface of the still strained film aside the wrapped tube.

Electronic Supplementary Material (ESI) for RSC Advances

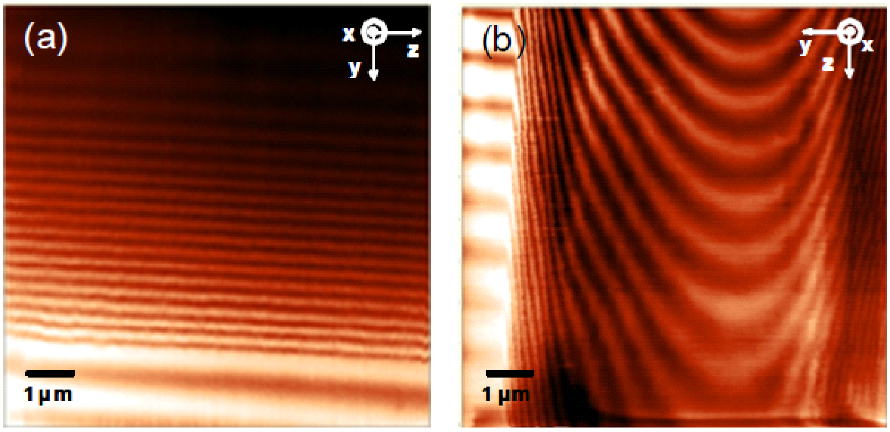

Figure 3 (color online) MFM images scanned at 500 Oe applied (a) parallel to the tube axis (z axis) and (b) parallel to tube diameter (along y axis). The lowermost part of Fig. 3(a) and the leftmost part of Fig. 3(b) show stripe domain patterns of the film still adhered to the substrate and next to rolled-up tube.

Being aware of the fact that in the MFM images generated during MFM tip scans, the radial gradient field is convoluted as the curvature of the surface of the tubes, we can estimate a period D_{exp} of approximately 1 μm for stripe-shaped domains observed in the more flat regions immediately aside of rolled-up tubes shown in Figures 3(a) and (b). Otherwise, a fine dense stripe structure is observed in the tube walls. Remembering that domain wall energy can be expressed as $\sigma = 2\pi(AK_u)^{1/2}$, with $K_u = 3.4 \times 10^6$ erg cm^{-3} (or 3.4×10^5 J m^{-3}) and exchange stiffness constant $A \sim 10^{-6}$ erg cm^{-1} (or 10^{-11} J m^{-1}), we obtain $\sigma = 12$ erg cm^{-2} (or 12×10^{-3} J m^{-2}) and $W^{\pm} = 0.53$ μm. This average $W^{\pm}$ values leads to a predicted period of 1.06 μm in quite well agreement with observed one. Figure 4 shows MFM images scanned at different magnetic field values applied along the tube axis. The period of stripes does not change significantly as function of the fields applied along the tube axis.

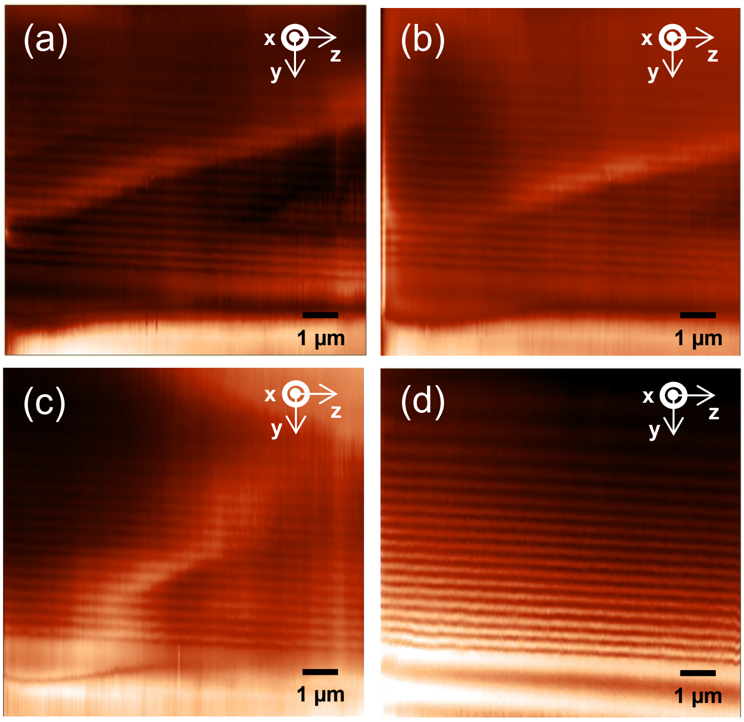

Figure 4: (color online) MFM images scanned in the same region of a rolled-up tube at different magnetic fields applied along the tube axis (z axis): (a) 0 Oe, (b) 100 Oe, (c) 300 Oe and (d) 500 Oe. All images areas are 10 μm x 10 μm.

To understand the weak field dependence of domain patterns shown in Figure 4 it is better to set aside the approach of Kittel and consider a more sophisticate model that explores in a more depth the stripe-shaped domains with straight domain walls in magnetic films with PMA [41]. Since the applied fields along tube axis are much smaller than anisotropy field (4 kOe), it is quite reasonable to assume that the deviations of the magnetization from the easy radial axis within the stripes can be neglected. Following the work of Kiselev *et al.* [41], a film of thickness L of unlimited extension in length with widths of domains polarized in the directions parallel (+) and antiparallel (–) given by $d^{\pm}$ will show a stripe pattern period of the domain structure $D = d^{+} + d^{-}$ in an effective bias field $H = H_z - 2\pi M$. The minimization of the magnetic density energy is given in terms of the parameters $p = 2\pi L/D$ and $q = (d^{+} - d^{-})/D$, which describe the balance between the domain wall and stray field energies. The minimization with respect to p and q yields the following equations for equilibrium values [41]:

$$p(u) = \frac{2}{u}\sqrt{1+\left(\frac{h}{h^{*}}\right)^{2}} \tag{1a}$$

$$q(u) = \frac{2}{\pi}\arcsin\left(\frac{h}{h^{*}}\right) \tag{1b}$$

where $u = (2/p)\cos(\pi q/2)$, $h = H/4\pi M_S$, and the parameter h^{*} is defined by the transition field into the saturated state ($p = 0$, $q = 1$), which means that the transition into the saturate state takes place by an infinite expansion of the domains with magnetization parallel to the applied field. In this case, domains with the antiparallel magnetization with respect to the applied field keep a finite size. According to this model, in the 'thin' film limit the domain sizes (d^{+}, d^{-}) change only slowly at low fields $h < h^{*}$ and an exponential growth of the size d^{+} sets in only close to the saturation field. Besides, the minority domain size d^{-} gradually decreases with increasing magnetic field and remains finite at the transition field. In this case, linear magnetization curves $M/M_S = h$ are expected in a broad range of magnetic field, resulting in an almost field-independent stripe-shaped domain patterns. For small fields compared to H_K values the domain patterns observed in Figure 4 are therefore consistent with this model.

In our case, we can easily obtain that p and q are close to zero (with $u \to 0.02$). Then, solutions for the equilibrium values of p at zero field ($q = 0$) yield a specific dependence of zero-field period D_0 on the layer thickness. The transition between a stripe-shaped perpendicular domain structure and uniform planar domains in a film with PMA of arbitrary thickness as a function of an in-plane applied field is expected to occur around anisotropy field H_K. Thus, measuring the critical field at which a stripe domains pattern disappears corresponds, apart from a correction term, to measure the local value of the anisotropy field H_K at the observation point [35]. Despite the critical field was not obtained in this work, we can determine a characteristic length $L_C = \sigma/2\pi M_S^{2}$, which describes the balance between domain wall and stray field energies. By taking the values above, we obtain L_C = 320 nm, leading to $L<L_C$ which implies that oblique domain walls do not exist, while straight domain walls exist for any thickness [41]. Therefore, straight domain walls running along the tube radius are expected.

Conclusions

In conclusion, we have fabricated rolled-up nanomembranes with self-organized magnetic domains radially aligned, which behaves as radially polarized cylindrical magnets due to perpendicular anisotropy. Basic magnetism considerations are in good agreement with the MFM observation. We hope that our present work could stimulate studies and application using with rolled-up tube geometry.

Acknowledgements

We thank financial support by the CNPq and Fundação Araucária (PRONEX Conv.118/2010 No.17386) Brazilian Agencies. Special thanks to REUNI/UFPR (J.Z.), CAPES/PRODOC (H.F.J), FAPEMIG (M. D. M. and S. O. P.) and Deutsche Forschungsgemeinschaft (C. M., within the research fellowship program, grant MU2766/3) for financial support.

References

1 T. C. Ulbrich, D. Makarov, G. Hu, I. L. Guhr, D. Suess, T. Schrefl and M. Albrecht, *Phys. Rev. Lett.* 2006, **96**, 077202.

2 J. M. Garcia, A. Asenjo, J. P. Sinnecker and M. Vazquez, *J. Magn. Magn. Mat.* 2000, **215**, 352.

3 Nielsch, F. J. Castaño, C. A. Ross, and R. Krishnan, *J. Appl. Phys.* 2005, **98**, 034318.

4 R. Cowburn and M. Welland, *Science* 2000, **287,** 1466.

5 S. Khizroev, M. Kryder, D. Litvinov and D. Thomson, *Appl. Phys. Lett.* 2002, **81**, 2256.

6 A. Goldstein, M. Gelb, P. Yager and C. A. Haberzettl, *Nanotechnology* 2002, **13**, R9.

7 O. G. Schmidt and K. Eberl, *Nature* 2001, **410**, 168.

8 V. Ya Prinz, V. A. Seleznev, A. K. Gutakovsky, A. V. Chehovskiy, V. V. Preobrazhenskii, M. A. Putyato and T. A. Gavrilova, *Physica E* 2000, **6**, 828.

9 G. S. Huang, Y. F. Mei, D. J. Thurmer, E. Coric and O. G. Schmidt, *Lab Chip*, 2009, **9**, 263.

10 S. Schulze, G. S. Huang, M. Krause, D. Aubyn, V. A. Bolaños Quiñones, C. K. Schmidt, Y. F. Mei and O. G. Schmidt, *Adv. Eng. Mater.*, 2010, **12**, B558.

11 H. X. Ji, X. L. Wu, Z. Fan, C. Krien, I. Fiering, Y. G. Guo, Y. F. Mei and O. G. Schmidt, *Adv. Mater.*, 2010, **22**, 4591.

12 C. C. Bof Bufon, J. D. C. Gonzalez, D. J. Thurmer, D. Grimm, M. Bauer and O. G. Schmidt, *Nano Lett.*, 2010, **10**, 2506.

13 C. C. Bof Bufon, J. D. A. Espinoza, D. J. Thurmer, M. Bauer, C. Deneke, U. Zschieschang, H. Klauk and O. G. Schmidt, *Nano Lett.*, 2011, **11**, 3727.

14 D. J. Thurmer, C. C. Bof Bufon, C. Deneke and O G Schmidt, *Nano Lett.*, 2010, **10**, 3704.

15 S. M. Harazim, V. A. Bolaños Quiñones, S. Sanchez and O. G. Schmidt, *Lab Chip*, 2012, **12**, 2649.

16 S. Mendach, R. Songmuang, S. Kiravittaya, A. Rastelli, M. Benyoucef and O. G. Schmidt, *Appl. Phys. Lett.*, 2006, **88**, 111120.

17 T. Kipp, H. Welsch, C. Strelow, C. Heyn and D. Heitmann, *Phys. Rev. Lett.*, 2006, **96**, 077403.

18 R. Songmuang, A. Rastelli, S. Mendach, C. Deneke and O. G. Schmidt, *Microelec. Eng.*, 2007, **84**, 1427.

19 E. J. Smith, S. Kiravittaya, Y. F. Mei, S. Sanchez and O. G. Schmidt, *Nano Lett.*, 2011, **11**, 4037.

20 E. Bermúdez-Ureña, Y. F. Mei, E. Coric, D. Makarov, M. Albrecht and O. G. Schmidt, *J. Phys. D: Appl. Phys.*, 2009, **42**, 055001.

21 C. Deneke, J. Schumann, R. Engelhard, J. Thomas, C. Müller, M. S. Khatri, A. Malachias, M. Weisser, T. H. Metzger and O. G. Schmidt, *Nanotechnology* 2009, **20**, 045703.

22 C. Müller, M. S. Khatri, C. Deneke, S. Fähler, Y. F. Mei, E. Bermúdez Ureña and O. G. Schmidt, *Appl. Phys. Lett.* 2009, **94**, 102510.

23 E. J. Smith, D. Makarov and O. G. Schmidt, *Soft Matter*, 2011, **7,** 11309.

24 E. J. Smith, D. Makarov, S. Sanchez, V. M. Fomin and O. G. Schmidt, *Phys. Rev. Lett.*, 2011, **107**, 097204.

25 F. Balhorn, S. Mansfeld, A. Krohn, J. Topp, W. Hansen, D. Heitmann and S. Mendach, *Phys. Rev. Lett.*, 2010, **104**, 037205.

26 I. Mönch, D. Makarov, R. Koseva, L. Baraban, D. Karnaushenko, C. Kaiser, K. F. Arndt and O. G. Schmidt, *ACS Nano*, 2011, **5**, 7436.

27 C. Müller, C. C. Bof Bufon, M. E. Navarro Fuentes, D. Makarov, D. H. Mosca and O. G. Schmidt, *Appl. Phys. Lett.*, 2012, **100**, 022409.

28 C. Müller, C. C. Bof Bufon, D. Makarov, L. E. Fernadez-Outon, W. A. A. Macedo, O. G. Schmidt and D. H. Mosca, *Nanoscale* 2012, **4**, 7155.

29 J. Schuhmann, K. G. Lisunov, W. Escoffier, B. Raquet, J. M. Broto, E. Arushanov, I. Mönch, D. Makarov, C. Deneke and O. G. Schmidt, *Nanotechnology*, 2012, **23**, 255701.

30 R. Streubel, J. Lee, D. Makarov, M Y Im, D. Karnaushenko, L. Han, R. Schafer, P. Fischer, S. K Kim and O. Schmidt, 2013, *Adv. Matter.* (doi: 10.1002/adma.201303003)

31 P. F. Garcia, *J. Appl. Phys.*, 1988, **63**, 5066

32 J. Zarpellon, H. Jaffrès, J. Frougier, C. Deranlot, J. M. George, D. H. Mosca, A. Lemaître, F. Freimuth, Quang Ha Duong, P. Renucci, and X. Marie, *Phys. Rev. B* 2012, **86**, 205314.

33 J. Lee, D. Suess, T. Schrefl, K. Hwan Oh and J.Fidler, *J. Magn. Magn. Mat.* 2007, **310**, 2445.

34 C. Kittel, *Phys. Rev.* 1946, **70**, 965.

35 A. Hubert and R. Schäfer, *Magnetic Domains* (Springer, Berlin, 1998).

36 E. P. Furlani, S. Reznik and A. Kroll, *IEEE Trans. Mag.* 1995, **31**, 844.

37 J. Escrig, P. Landeros, D. Altbir and E.E. Vogel, *J. Magn. Magn. Mater.* 2007, **310**, 2448.

38 P. Landeros, S. Allende, J. Escrig, E. Salcedo, D. Altbir, and E. E. Vogel, *Appl. Phys. Lett.* 2007, **90**, 102501.

39 J. Escrig, P. Landeros, D. Altbir, E.E. Vogel and P. Vargas, *J. Magn. Magn. Mater.* 2007, **308**, 233.

40 J. Escrig, J. Bachmann, J. Jing, M. Daub, D. Altbir, and K. Nielsch, *Phys. Rev. B* 2008, **77**, 214421.

41 N. S. Kiselev, I. E. Dragunov, A. T. Onisan, U. K. Rößler, and A. N. Bogdanov, *Eur. Phys. J. Special Topics* 2008, **158**, 119.